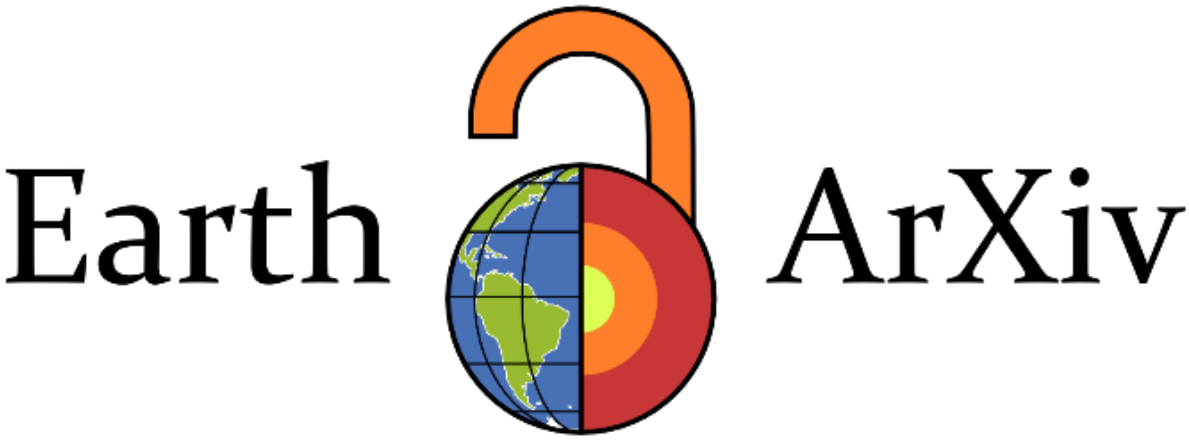

Model-Free Relative Permeability Estimation and Oil Recovery Prediction in Reservoir Rocks from Capillary Pressure Curves

Elena M. Avraham
Kuban State Agrarian University named after I.T. Trubilin,
Krasnodar, Russian Federation
e-mail: av.el3@yandex.com

Abstract

This paper presents and validates a model-free method for predicting the relative permeability and oil recovery of reservoir rocks directly from the shape of the capillary pressure curve, tested against real reservoir core, digital rock models, and a large soil-hydraulic dataset. Relative permeability is the key saturation function governing production forecasts, water cut, and oil recovery in reservoir simulation, yet its direct measurement requires costly special core analysis (SCAL), while capillary pressure curves are obtained routinely and at low cost from mercury injection porometry (MICP) or capillarimetry. We introduce a spectral relative-permeability exponent, computed as the mean logarithmic slope of the Mualem integral kernel, requiring no selection or fitting of a parametric capillary pressure model; the classical Brooks–Corey exponent emerges as its limiting special case. On real Berea sandstone reservoir core from two independent published datasets — oil as the wetting phase and gas as the non-wetting phase — the method reproduces the measured relative permeability with a logarithmic coefficient of determination of 0.995 and 0.978, respectively, using a single calibrated scale factor and no fitted shape parameters. On four digital rock models (Bentheimer and Doddington sandstones, Estaillades and Ketton limestones), the exponent predicted from capillary pressure alone agrees with pore-network flow simulation on the same segmented pore geometry, with a logarithmic coefficient of determination of 0.82–0.98. Statistical robustness is further confirmed on a combined dataset of 283 real capillary pressure/relative permeability pairs, where the method matches the accuracy of the best-fitting parametric models without fitting any shape parameters. Beyond validation, the method quantifies its own fundamental limit: the residual gap to the best achievable power-law fit is shown to be structural, linked to pore-space connectivity, rather than random noise. A closed-form analytical expression for the sensitivity of the water-free oil recovery factor to the exponent enables a confidence interval for oil recovery to be constructed from a single capillary pressure curve, and an economic criterion is formulated for the cost-effectiveness of direct flow experiments, expressed in barrels of movable oil. The results provide a laboratory- and pore-scale-validated basis for core analysis optimization and for populating geological and reservoir simulation models with saturation functions at scale, particularly relevant for hard-to-recover reserves and polymodal carbonate reservoirs.

Keywords: digital rock physics, oilfield development, oil recovery prediction, Mualem model, Brooks–Corey model, saturation functions, mercury injection porosimetry, MICP, SCAL, relative permeability

Introduction

The movement of multiphase fluids in the reservoir rock of an oil and gas deposit, as in any porous medium, is fully governed by two state functions. The capillary pressure curve $P_c(S)$ relates capillary pressure to the saturation of the wetting phase S, while relative permeability $k_r(S)$ defines the fraction of absolute permeability available to a given phase at a given saturation. The pair $\{P_c, k_r\}$ closes the system of two-phase flow equations — including the Buckley–Leverett model and the multiphase flow equations used in reservoir development problems — and thereby governs the prediction of production rates, water breakthrough time, water cut, and the oil recovery factor (RF). The accuracy with which this pair is determined directly controls the accuracy of the predicted development performance indicators.

A fundamental asymmetry in cost and measurement time exists between the two functions. The P_c curve is obtained at relatively moderate cost using mercury injection capillary pressure (MICP), centrifuge, or porous-plate (capillarimetry) methods, and as a result it is available in large volumes in petrophysical practice. Measuring k_r, by contrast, requires lengthy steady-state or unsteady-state core-flooding experiments carried out within special core analysis (SCAL), which are incomparably more expensive and time-consuming. This gives rise to the classical problem of petrophysics: predicting relative permeability k_r from P_c curves without conducting resource-intensive flow experiments. Predicting k_r from P_c is needed at the field evaluation stage, when specifying saturation and relative permeability functions in reservoir simulation models, during history matching, and when screening waterflooding scenarios, enhanced oil recovery (EOR) methods, and geological CO_2 storage projects.

In practice, this prediction task faces three unresolved problems. The first concerns the arbitrariness of the choice of parametric model: standard fitting of Brooks–Corey or van Genuchten approximations to the measured P_c curve, followed by computing $k_r$via the Burdine or Mualem method, introduces a non-physical dependence of the result on the mathematical form of the approximation. The second stems from the absence of a quantitative measure of confidence: it remains unknown what fraction of the variability in k_r is, in principle, determined by the P_c curve, making it impossible to assess either the prediction error or the value of a direct flow measurement. The third is the lack of a rational rule for prioritizing costly experiments: no quantitative relationship has been established between the error in predicting $k_r$and the error in predicting oil recovery. Taken together, these problems shift the task from the engineering-level choice of a more accurate correlation to the epistemic-level question of the upper bound of information that can be extracted from P_c.

This need for prediction gave rise to a family of capillary-based permeability models (Purcell, 1949; Burdine, 1953; Childs and Collis-George, 1950; Mualem, 1976), in which k_r is computed as a saturation-weighted integral of power-law functions of capillary pressure — either $1/P_c$ (Mualem's model) or $1/P_c^2$ (the Purcell and Burdine models). In practice, the calculation is carried out not on the measured

curve itself but on its parametric approximation (Brooks and Corey, 1964; van Genuchten, 1980), fitted with two to four parameters. All of these models reduce to the power-law limit $k_r \sim S_e^n$, in which the exponent $n$is expressed through the pore-size distribution index $\lambda$and the tortuosity parameter τ. The specific form of the expression for $n$differs from model to model. For one and the same measured P_c curve, different approximations yield different values of k_r, and it remains unclear what part of the discrepancy reflects the physics of the medium and what part is due to the arbitrariness of model choice.

Over the past decade, the reconstruction of relative permeability from available petrophysical data has advanced considerably through machine learning methods and integral correlations. Neural-network models have been proposed for predicting k_r directly from mercury injection capillary pressure curves (Duan et al., 2024), as well as for the joint estimation of k_r and P_c in tight reservoirs from routinely measured parameters using physics-informed neural networks (Ji et al., 2023). An approach has been developed that adapts k_r functions with explicit account for interfacial tension (Moodie and McPherson, 2024). In parallel, digital core analysis combined with deep learning is being applied to predict storage and flow (petrophysical) properties from three-dimensional images of the pore space. This line of work includes quantitative uncertainty estimation for such predictions (Liu et al., 2023; Meng et al., 2023), as well as interpretable reconstruction of porosity and permeability in tight sandstones from a set of petrophysical attributes (Cao et al., 2025). These approaches demonstrate high accuracy, but rely either on representative training datasets or on detailed digital pore geometry. Importantly, none of them answers the question of the upper bound of predictability: what fraction of the variability in k_r is, in principle, determined by the shape of the P_c curve.

A physically grounded alternative to these approaches is direct pore-scale flow modeling, which requires no training data and relies on the actual pore space geometry. Hybrid schemes have been proposed for computing $k_r$that combine pore-network modeling (PNM) with the volume-of-fluid (VOF) method (Lanetc et al., 2024), as well as multiscale and dual-network models that account for the unresolved microporosity of carbonates (Foroughi et al., 2024; Zhao et al., 2025). The accuracy of such models depends largely on the correct extraction of the pore network from images (Liu Y. et al., 2022). A separate line of research quantitatively relates the shape of saturation functions to the structure and wettability of the pore space: the influence of bimodal pore-size distributions on k_r and P_c has been demonstrated, together with an uncertainty assessment (Zhang et al., 2023), as has the influence of heterogeneity and capillary discontinuities on effective saturation functions — both through numerical upscaling of digital core analysis data (Aslannezhad et al., 2024; Matthai and Tran, 2023) and on real core material from carbonate reservoirs (Al-Dujaili et al., 2023). The pore-scale physics underlying the formation of $k_r$curves has been investigated using the lattice Boltzmann method (LBM) (Bagherabadi et al., 2025). At the same time, despite their physical transparency, the methods listed above remain computationally expensive and require high-quality images.

Critical-path analysis provides a quantitative link between the width of the pore-size distribution and the exponent of k_r. Ghanbarian and co-authors (Ghanbarian et al., 2017) estimate the relative permeability of the wetting phase k_{rw} by approximating the pore-size distribution with a log-normal density $f(r)$and computing k_{rw} from the expression

$$k_{rw} = \left(\frac{r_c(S_w)}{r_c(S_w = 1)} \right)^{\alpha}$$

in terms of the critical percolation radius r_c, transitioning to a universal power law near the critical saturation. Here α denotes the critical percolation conductivity exponent, related to the index t of percolation theory. The model's input and fitted parameters include the measurable porosity $\phi$and critical saturation S_{wc}, together with fitted geometric characteristics — a pore-channel shape factor and the percolation exponent α. The width σ of the log-normal distribution, however, corresponds not to a directly measured pore-size distribution but to a distribution fitted to the shape of the P_c curve, which is a significant limitation of the method when applied to real polymodal reservoirs.

Thus, the literature review reveals four fundamental unresolved problems.

- Parametric capillary models and machine learning methods are model-dependent, in the sense that their output is determined by the choice of parametric form used to approximate P_c, or by the architecture of the trained model, rather than solely by the physical content of the P_c curve. Pore-network-based modeling, along with methods built on the lattice Boltzmann equations, are free of this parametric-form ambiguity, but carry their own model dependence of a different kind: geometric idealization assumptions in pore representation (PNM), and the effects of tomographic resolution and boundary conditions (LBM). Within the scope of existing approaches, it is impossible to separate the contribution of any of these assumptions from the true physics of the medium.

- None of the existing approaches establishes an upper bound on the predictability of k_r from P_c. It remains unknown what fraction of the variability in k_r is, in principle, determined by the shape of the P_c curve, and what fraction is due to information about pore-space connectivity and structure that is inaccessible from capillary measurements alone. Without an answer to this question, no prediction can be assigned a quantitative accuracy estimate.

- The nature of the irreducible residual between the best prediction of k_r from P_c and the exponent obtained by direct fitting to experimental k_r data has not been systematically investigated: it is unknown whether this residual is random noise or carries physically interpretable information about pore-space structure that can be partially recovered from available petrophysical descriptors.

- There is no quantitative relationship between the error in predicting k_r and the error in predicting oil recovery: no analytical expression has been derived that translates the error in the estimated relative-permeability exponent into an error in

the oil recovery factor, and no rational economic criterion has been formulated for the cost-effectiveness of expensive direct flow experiments to determine k_r.

The present work is aimed at a comprehensive solution of the problems listed above. Its objectives are as follows.

- To derive a closed-form analytical formula for the effective relative-permeability exponent n_M as a spectral moment of the Mualem kernel, computed directly from the measured P_c curve without selecting or fitting any capillary pressure model, and to show that the Brooks–Corey model is a limiting special case of this formula corresponding to the limit of perfect correlation, thereby providing a physical explanation for its long-standing empirical success.

- To establish, using representative independent datasets of real data (soils, digital rock models, and laboratory reservoir core), a quantitative predictability limit for k_r from P_c in terms of the logarithmic coefficient of determination $R^2_{\log}$, and to rigorously verify that the model-free exponent n_M attains this limit without fitting any shape parameters.

- To carry out a systematic analysis of the structure of the residual $r = n_{\text{opt}} - n_M$ and to establish whether this residual is random noise or carries physically interpretable information about pore-channel connectivity that can be partially recovered from grain-size (granulometric) descriptors.

- To obtain a closed-form analytical expression for the sensitivity of the oil recovery factor over the water-free production period to the exponent n, for a consistent two-phase relative-permeability system $\{k_{rw}, k_{ro}\}$ based on the Mualem model; to use it to construct a confidence interval for oil recovery directly from a single P_c curve; and to formulate a quantitative, scale-dependent criterion for the cost-effectiveness of direct flow experiments to determine k_r, expressed in barrels of movable (mobile) oil.

Materials and Methods

Consider a porous-medium sample for which the capillary pressure curve $P_c(S)$ is known, measured over the saturation interval $[S_{\min}, S_{\max}]$. The task is to construct a predictor for k_r that relies exclusively on the shape of the P_c curve, up to a scale factor, and to quantitatively characterize its accuracy and its fundamental limit. The predictor is defined in power-law form:

$$k_r(S_e) = A\, S_e^{\,n_M},\ S_e = \frac{S - S_{wr}}{1 - S_{wr} - S_{or}} \in [0,1], \tag{1}$$

where S_e is the effective saturation, S_{wr} and S_{or} are the residual saturations of the wetting and non-wetting phases, n_M is the model-free spectral exponent, computed from P_c as the slope of the Mualem integral kernel in logarithmic space, and A is the single calibrated parameter, equivalent to one conductivity measurement (for example, the absolute permeability K_{abs}, which sets the scale via $k = K_{abs} \cdot k_r$). No

shape parameters are fitted to the k_r data.

The derivation of the formula for the exponent n_M is based on the Mualem integral representation for the relative permeability of the wetting phase:

$$k_M(S_e) = S_e^{\tau}\left[\frac{\int_0^{S_e}\frac{dS'}{P_c(S')}}{\int_0^{1}\frac{dS'}{P_c(S')}}\right]^2 = S_e^{\tau}\hat{I}^2(S_e),$$

where

$$\hat{I}(S_e) = \frac{I(S_e)}{I(1)}$$

denotes the normalized capillary-conductivity integral. The logarithm of this functional takes the form

$$\ln k_M = \tau \ln S_e + 2\ln \hat{I}\,(S_e).$$

It follows that the contribution of tortuosity is governed by the constant slope τ, while the influence of the shape of the capillary pressure curve is contained entirely in the logarithmic slope of the function $\hat{I}(S_e)$. The model-free spectral exponent is therefore defined as the mean logarithmic slope of the Mualem functional,

$$n_M = \frac{d\ \ln \bar{k}_M}{d\ \ln S_e} = \tau + 2\frac{d\ \ln \bar{\hat{I}}}{d\ \ln S_e},$$

where the derivative is understood in the sense of a mean logarithmic slope and is subsequently computed from the experimental data as the slope of a weighted linear regression of $\ln k_M$ on $\ln S_e$.

The algorithm for computing the exponent n_M from experimental data consists of four deterministic steps. First, the curve is normalized to the effective saturation S_e, after which the capillary conductivity $Q(s) = 1/P_c(s)$ is introduced, together with the Mualem integral $I(S_e) = \int_0^{S_e} Q\,ds$, normalized as $\tilde{I}(S_e) = I(S_e)/I(1)$. Since the experimental data cover only the interval $[S_{\min}, S_{\max}]$, while the integral requires integration from zero, the segment $[0, S_{\min}]$ is reconstructed using a local power law $Q \sim S_e^{q}$, fitted to the curve points in the low-saturation region ($S_e \to 0$):

$$\int_0^{S_{\min}} Q\ ds = \frac{Q(S_{\min})\,S_{\min}}{q+1}, \tag{2}$$

which follows from the power law $Q \sim S_e^q$ upon integration from 0 to $S_{\min}$. Next, the Mualem integral kernel $k_M(S_e) = S_e^\tau\,[\tilde{I}(S_e)]^2$ is constructed using the canonical tortuosity exponent $\tau = 0.5$, and in logarithmic coordinates $x = \ln S_e$ the slope is estimated by weighted least squares, yielding the sought exponent:

$$n_M = \frac{\mathrm{Cov}_\mu(\ln k_M, x)}{\mathrm{Var}_\mu(x)}, \qquad x = \ln S_e. \tag{3}$$

Finally, the scale factor A in the formula $k_r = A\,S_e^{n_M}$ is calibrated from a single conductivity measurement. The baseline measure is taken to be uniform in effective saturation ($d\mu = dS_e$). An alternative logarithmic measure, $d\mu = d\ln S_e$, was tested separately and has a negligible effect on the result. All operations of the computational algorithm (the integral quadrature and the weighted log–log regression) are linear and well-conditioned, so the estimator requires no nonlinear optimization and contains no free shape parameters. Note that the exponent n_M is invariant under multiplicative rescaling of P_c (in particular, under conversion of MICP data to the reservoir fluid system via the Young–Laplace relation through $\sigma\cos\theta$), since it is determined solely by the shape of the curve in logarithmic coordinates.

Prediction accuracy is evaluated using the logarithmic coefficient of determination, which correctly accounts for variation in $k_r$spanning several orders of magnitude:

$$R^2_{\log} = 1 - \frac{\sum_i (\ln k_{r,i}^{\mathrm{meas}} - \ln k_{r,i}^{\mathrm{mod}})^2}{\sum_i (\ln k_{r,i}^{\mathrm{meas}} - \overline{\ln k_r^{\mathrm{meas}}})^2}. \tag{4}$$

The linear coefficient of determination R^2 is also reported for comparison with literature data; however, its value is determined predominantly by points at high saturation, where $k_r \to 1$, which overstates the quality of the prediction in the low-k_r region — the region most significant for engineering calculations.

The model-free exponent n_M is compared against the canonical capillary models — Brooks–Corey–Mualem, Burdine, and Mualem–van Genuchten — as well as against the two-parameter empirical predictability ceiling n_{opt}. The comparison includes the Brooks–Corey–Mualem exponent

$$n_{BC} = \tau + 2 + \frac{2}{\lambda},$$

the Burdine exponent

$$n = 3 + 2/\lambda,$$

the closed-form Mualem–van Genuchten expression with parameter $m = \lambda/(\lambda + 1)$:

$$k_{rw} = S_e^{1/2}\left[1 - \left(1 - S_e^{1/m}\right)^m\right]^2, \quad m = \frac{\lambda}{\lambda + 1} \tag{5}$$

and the freely fitted power-law exponent n_{opt}. The latter is determined by a two-parameter fit (scale factor and exponent) directly to the experimental k_r data points and serves as the upper bound on the accuracy achievable within the class of power-law relationships. The difference $n_{\mathrm{opt}} - n_M$ defines a measure of the predictability limit. The reliability of the accuracy and limit estimates is established by resampling (the bootstrap method): confidence intervals are constructed for the median $R^2_{\log}$ and the median exponent n_M.

In analyzing the relationships between the residual and the physical and textural properties of the medium, the Benjamini–Hochberg procedure is applied, and the contribution of texture is separated from the trivial dependence via partial correlation controlling for the index λ. The recoverability of the residual from descriptors is tested by nested cross-validation, with feature selection performed within the training subsample, and by permutation tests of the significance of the quality gain on the held-out sample. The transferability of the residual model between independent data sources is assessed by cross-validation under the "A"→"B" and "B"→"A" schemes. In addition, the skewness and kurtosis of the $\ln P_c$ distribution are computed for each curve: the affine relationship between $\ln P_c$ and $\ln S_e$ in the Brooks–Corey model defines an invariant point in the skewness–kurtosis plane (Tyler and Wheatcraft, 1990; Meer and Weeks, 2024), and the distance to this point is used as a fit-free diagnostic of how closely a curve approaches power-law form.

The engineering implications of replacing measured k_r with the model-free prediction are evaluated by computing two-phase displacement using Buckley–Leverett theory (Buckley and Leverett, 1942) with the Welge graphical construction (Welge, 1952). The fractional-flow function of the displacing phase (neglecting capillary and gravitational terms)

$$f_w(S_w) = \left[1 + \frac{\mu_w}{\mu_o}\,\frac{k_{ro}(S_w)}{k_{rw}(S_w)}\right]^{-1} \tag{6}$$

determines the frontal saturation and the average saturation behind the front, from which the dependence of the recovery factor on the volume of water injected is reconstructed. To quantitatively link the error in the relative-permeability exponent to the error in the oil recovery prediction, we derive a closed-form sensitivity of the water-free recovery factor to the exponent n. The frontal saturation $S_{e,f}$ is given by the Welge tangent construction from the origin, $f_w'(S_{e,f}) = f_w(S_{e,f})/S_{e,f}$, and the water-free recovery factor, expressed as a fraction of movable oil, is $RF_{bt} =$

$S_{e,f}/f_w(S_{e,f})$. Since the front realizes a stationary point of RF with respect to saturation (the envelope theorem: $\partial(S_e/f_w)/\partial S_e = 0$ at the point of tangency), the total derivative reduces to the partial derivative at fixed $S_{e,f}$. For a consistent two-phase relative-permeability system based on the Mualem model, $k_{rw} = S_e^n$, $k_{ro} = (1 - S_e)^\tau \left(1 - S_e^{1+p}\right)^2$, with $p = 1/\lambda$ this gives

$$\frac{\partial RF_{bt}}{\partial n} = RF_{bt}\left(1 - f_{w.f}\right)\left[\ln\frac{1}{S_{e,f} + a_{o,f}}\right], \tag{7}$$

$$a_{o,f} = \frac{S_{e,f}^{1+p}\ln\left(1/S_{e,f}\right)}{1 - S_{e,f}^{1+p}}, \qquad p = \frac{1}{\lambda} = \frac{2n - \tau - 2}{2},$$

where the term $a_{o,f}$ represents the contribution of the coupled oil-phase permeability. When k_{ro} is held fixed, this term vanishes. All of the quantities involved are extracted from the standard Welge construction and require no additional data. The dimensionless water-free injection time $t_{D,bt}$ inherits the same sensitivity:

$$\frac{\partial t_{D,bt}}{\partial n} = (1 - S_{wc} - S_{or})\,\frac{RF_{bt}}{\partial n}.$$

The error in the oil recovery prediction incurred by replacing the measured exponent with the model-free one is estimated as

$$\Delta RF \approx \left|\frac{\partial RF_{bt}}{\partial n}\right| \cdot |\, r \,|,\ r = n_{\mathrm{opt}} - n_M.$$

Verification of the method is carried out exclusively on real experimental data: published laboratory curves, an open database of soil hydraulic properties, segmented micro-CT models of rocks, and oil-reservoir core with matched measurements of both state functions.

Dataset A (literature curves). Published matched pairs of P_c and k_r for sands, loams, silts, and clays (sources: Brooks and Corey, 1964; Mualem, 1976; Tuli and Hopmans, 2003; Assouline and Or, 2013). After quality control, 30 samples remain in the dataset.

Dataset B (UNSODA). The UNSODA database of unsaturated soil hydraulic properties (Nemes et al., 2001). After quality control, the combined sample contains ≈283 P_c/k_r pairs. The moment-based exponent is validated on all 283 pairs; the engineering calculation is carried out on 245 UNSODA samples with a complete set of descriptors. This dataset forms the primary statistical basis of the study, owing to its size and its broad coverage of textural classes.

Dataset C (digital rocks). Four segmented micro-CT models (Imperial College repository (Blunt et al., 2013; Andrä et al., 2013)) of order 1000^3 voxels: Bentheimer ($\phi = 21.7\%$) and Doddington ($\phi = 19.6\%$) sandstones, and Estaillades ($\phi = 12.7\%$) and Ketton ($\phi = 13.3\%$) limestones, with porosity given for the segmented (resolved) pore space. Four representative-elementary-volume (REV) subvolumes (edge length 150–250 voxels) were extracted from each model, giving 16 subvolumes in total. Dataset C provides a direct pore-scale test of the proposed equivalence, since it allows P_c, k_r, and topological descriptors to be computed independently on one and the same pore-space geometry (Valvatne and Blunt, 2004).

Dataset D (oil-reservoir core, wetting phase). A matched pair of P_c and $k_r$curves for a consolidated Berea sandstone sample (absolute permeability $K = 107$ mD $\approx 1.06 \times 10^{-13}$ m^2, porosity $\phi = 17.7\%$), published in the classic work of Richardson et al. (1952) and digitized from Fig. 1 of that paper (26 P_c points and 46 $k_r$points). The measurements correspond to a gas–oil drainage regime in which oil serves as the wetting phase, so the relative permeability is attributed to the oil phase. Dataset D contains real oil-reservoir core with direct laboratory measurement of both state functions and therefore provides a representative test of the model-free prediction as applied to the target object of the present study. Since both curves pertain to the same sample, they are assigned a single effective saturation, $S_e = (S - S_{or})/(1 - S_{or})$, with a common residual saturation S_{or}, which ensures the comparability of the exponents extracted from P_c and from k_r on a common scale.

Dataset E (oil-reservoir core, non-wetting phase). A matched pair of P_c and $k_r$curves for a Berea sandstone sample under gas/water drainage displacement, published by Pini and Benson (2013) and digitized from Table 2 and Fig. 6 of that paper (6 $P_c$points and 6 $k_r$points). Unlike Dataset D, where relative permeability is attributed to the wetting (oil) phase, here the permeability of the non-wetting phase (gas) is measured, which allows the transferability of the model-free exponent to be tested on the complementary flow path. Both state functions were obtained simultaneously on the same sample by the steady-state method with X-ray CT monitoring of saturation, so, as in Dataset D, a single effective saturation is adopted for them. For the non-wetting phase, the predictor is written in terms of $1 - S_e$, where $S_e = (S_w - S_{wr})/(1 - S_{wr})$. Dataset E complements Dataset D, extending the verification from a single flow phase to both.

Results

The proposed model-free spectral exponent $n_M = \tau + 2\beta$, with the exact factorization

$$n_M = \tau + 2\rho_{xy}\sigma_y/\sigma_x, \qquad x = \ln S_e, \qquad y = \ln \tilde{I}, \tag{8}$$

where $\beta = \rho_{xy}\,\sigma_y/\sigma_x$ is the slope of the regression of $\ln \tilde{I}$ on $\ln S_e$, moves the problem out of the plane of comparing individual models and into the plane of

information analysis. It measures what fraction of the variability in relative permeability is, in principle, determined by the shape of the capillary pressure curve, and thereby sets the upper bound for any prediction of k_r from P_c. Within this construction, the Brooks–Corey model turns out to be a limiting special case, corresponding to perfect linear correlation $\rho_{xy} = 1$, at which the dependence of $\ln \tilde{I}_M$ on $\ln S_e$ is exactly linear and the scale part of the factorization equals exactly $1 + 1/\lambda$. The Mualem integral projects an arbitrary P_c curve onto the subspace of power-law relationships in logarithmic coordinates, of which the Brooks–Corey model is the limiting case at $\rho_{xy} = 1$.

The equivalence of the model-free exponent n_M and the parametric exponent of the Brooks–Corey model is verified on a sequence of independent datasets. In the first stage of validation, the exponent is compared against the canonical models on a large soil dataset. On the UNSODA dataset (283 pairs, of which 245 have a complete set of descriptors), the median prediction quality $R^2_{\log} \approx 0.82$ is statistically indistinguishable from the Brooks–Corey and Burdine values, as evidenced by overlapping 95% bootstrap confidence intervals, with the exponent achieved without selecting or fitting a retention model, at the cost of a single calibrated parameter — the scale factor A.

In the second stage, these findings are validated on reservoir rocks. For a reservoir sandstone sample widely used in the literature as a reference benchmark (Gao et al., 2020), the model-free exponent $n_M = 3.624$ reproduces the analytical Brooks–Corey exponent $n_{BC} = 3.556$ with a discrepancy of $|\Delta| = 0.068$ (about 1.9%), which lies within the margin of error. Critically, the exponent n_M was computed solely from the shape of the primary-drainage P_c curve — not a single experimental k_r point was involved in its determination — which gives the test a predictive, rather than a post hoc, character.

The third stage is a paired test on a single piece of reservoir core, in which both state functions were measured independently on the same physical sample. For the classic dataset of Richardson, Kerver, Hafford, and Osoba [31] (Berea sandstone, $K = 107$ mD, gas–oil drainage regime with oil as the wetting phase), using a common residual saturation $S_{or} = 0.20$, the exponent recovered solely from the capillary pressure curve is $n_M = 4.26$. The exponent freely fitted to the measured k_r points is $n_{\text{opt}} = 4.03$, and the parametric Brooks–Corey estimate gives $n_{BC} = 3.99$ at $\lambda = 1.34$. The discrepancy $|n_M - n_{\text{opt}}| = 0.23$ corresponds to a structural residual $r = -0.23$; nevertheless, the $k_r$prediction based on the exponent n_M, with a single calibrated scale factor A, attains $R^2_{\log} = 0.995$, practically indistinguishable from the two-parameter ceiling $R^2_{\log} = 0.999$. Thus, the exponent extracted solely from the shape of P_c reproduces the independently measured relative permeability on real reservoir core, closing the direct verification of the entire prediction chain for the target class of media.

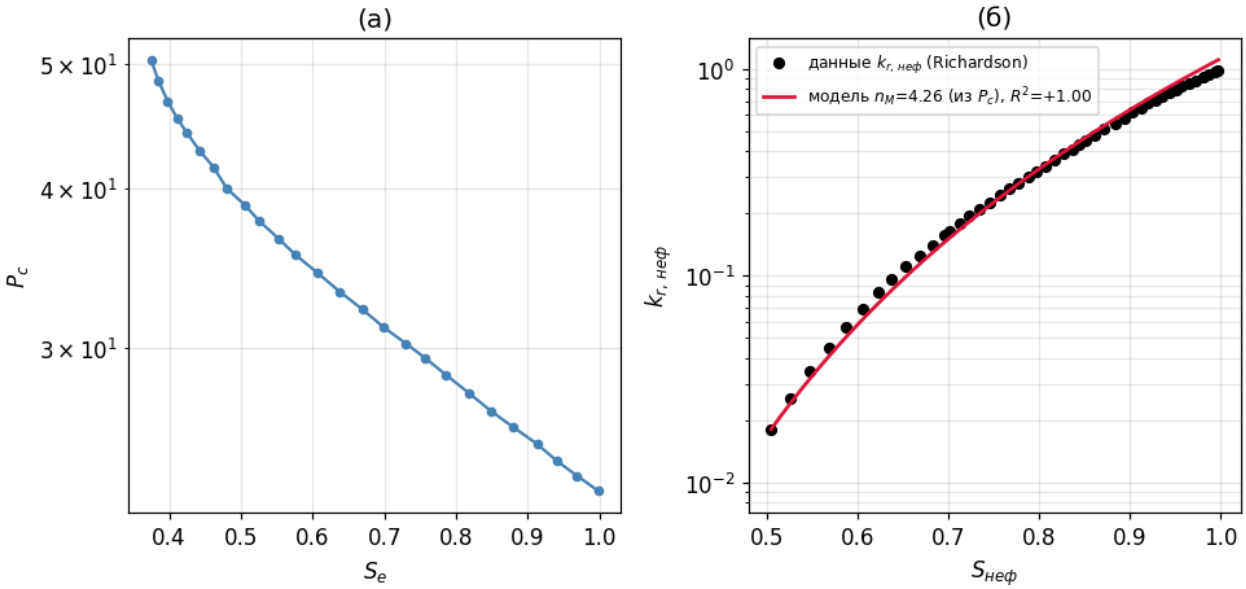

Figure 1. Paired verification of the model-free exponent on real Berea sandstone reservoir core ([31], $K = 107$mD, $\phi = 17.7\%$, gas–oil drainage, oil-wet). Both state functions were measured independently on the same sample. A common residual saturation $S_{or} = 0.20$defines a single effective-saturation scale $S_e = (S - S_{or})/(1 - S_{or})$for both $P_c$and k_r. **(a)** Drainage capillary pressure curve (26 points), from which the exponent $n_M = 4.26(\lambda = 1.34)$ is computed. **(b)** Oil relative permeability (46 points): solid line — prediction from the model-free exponent $n_M$with a single calibrated scale factor ($R^2_{\log} = 0.995$); dashed line — exponent $n_{opt} = 4.03$freely fitted to the $k_r$points ($R^2_{\log} = 0.999$). The agreement between the prediction and the independent measurement confirms the predictive, rather than post hoc, character of the estimate.

An additional test of the model-free predictor was carried out on a matched pair of P_c and k_r curves measured on a single Berea sandstone sample under drainage displacement in a gas–water system [32]. Unlike Dataset D, where permeability is attributed to the wetting (oil) phase, here the permeability of the non-wetting phase is measured, which allows the applicability of the model-free method for estimating n_M to be tested for both flow phases. For the non-wetting phase, the governing formula takes the form:

$$k_{r,nw}(S_e) = A\,(1 - S_e)^{\,n_M}, \;\; S_e = \frac{S_w - S_{wr}}{1 - S_{wr}}.$$

where $(1 - S_e)$ is the effective saturation of the non-wetting phase, and the residual water saturation $S_{wr} = 0.342$ is determined from a Brooks–Corey fit of the P_c curve and was not optimized. The exponent $n_M = 3.26$, computed from the measured $P_c$curve, differs from the canonical Brooks–Corey–Mualem value $n_{BC} = 3.29$ (at $\lambda = 2.52$) by only $|\,\Delta\,| = 0.03$, confirming the validity of the developed model-free approach. Upon calibration of the single scale factor A, the governing formula reproduces the measured non-wetting-phase relative permeability with a logarithmic coefficient of determination $R^2_{\log} = 0.978$. The predictability ceiling, obtained by

direct regression on the experimental k_r points, is $n_{\text{opt}} = 2.91$ at $R^2_{\log} = 0.992$. The gap between the model-free prediction and the ceiling in the $R^2_{\log}$ metric is 0.014, and the structural residual is $r = n_{\text{opt}} - n_M = -0.35$. The negative sign of the residual indicates that the model-free exponent systematically overestimates the optimal one, which is physically consistent with the non-wetting phase preferentially flowing through large, centrally located pores, whose permeability declines more slowly than predicted by the capillary structure. The closeness of n_M and n_{BC} and the high prediction accuracy for the non-wetting phase, together with the results for the wetting phase on the Richardson et al. data ($n_M = 4.26$, $R^2_{\log} = 0.995$, $r = -0.23$), confirm the applicability of the model-free method to both flowing phases, with a structural residual $| r | < 0.4$.

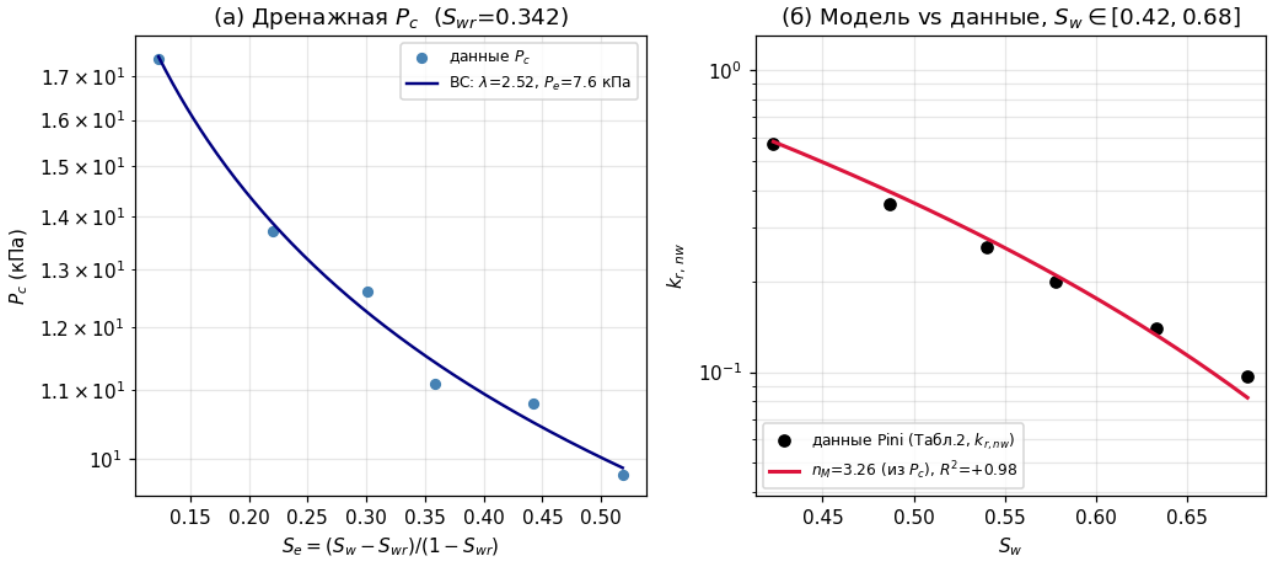

Figure 2. Validation of the model-free spectral exponent $n_M$on a Berea sandstone sample (N_2/water, drainage), based on data from Pini and Benson [32]. **(a)** Drainage capillary pressure curve $P_c$as a function of the effective water saturation $S_e = (S_w - S_{wr})/(1 - S_{wr})$ at $S_{wr} = 0.342$; solid line — Brooks–Corey fit ($\lambda = 2.52$, $P_e = 7.61$kPa). **(b)** Non-wetting-phase relative permeability $k_{r,nw}$: points — experimental data [Pini and Benson, 2013, Table 2]; solid line — model-free prediction $k_{r,nw} = A\,(1 - S_e)^{n_M}$with exponent $n_M = 3.26$extracted from the $P_c$curve and a single calibrated scale factor $A(R^2_{\log} = 0.978)$.

The fourth stage supplements these benchmark points with direct pore-network modeling on four lithologies (Bentheimer and Doddington sandstones, Estaillades and Ketton limestones; Dataset C). For each rock, a representative REV-scale subvolume was analyzed, having passed quality control on both state functions and possessing a non-degenerate index $\lambda \leq 5$. The model-free exponent $n_M$reproduces the analytical Brooks–Corey–Mualem exponent n_{BC} in all four cases, $| n_M - n_{BC} | \leq 0.20$ (mean absolute error, MAE = 0.13), and the prediction $k_{rw} = A\,S_e^{n_M}$ agrees with the permeability independently simulated on the same network at $R^2_{\log} =$ 0.82–0.98. Since P_c and k_{rw} are computed on identical pore geometry, this test

constitutes a self-consistency check of the model at the pore/rock scale.

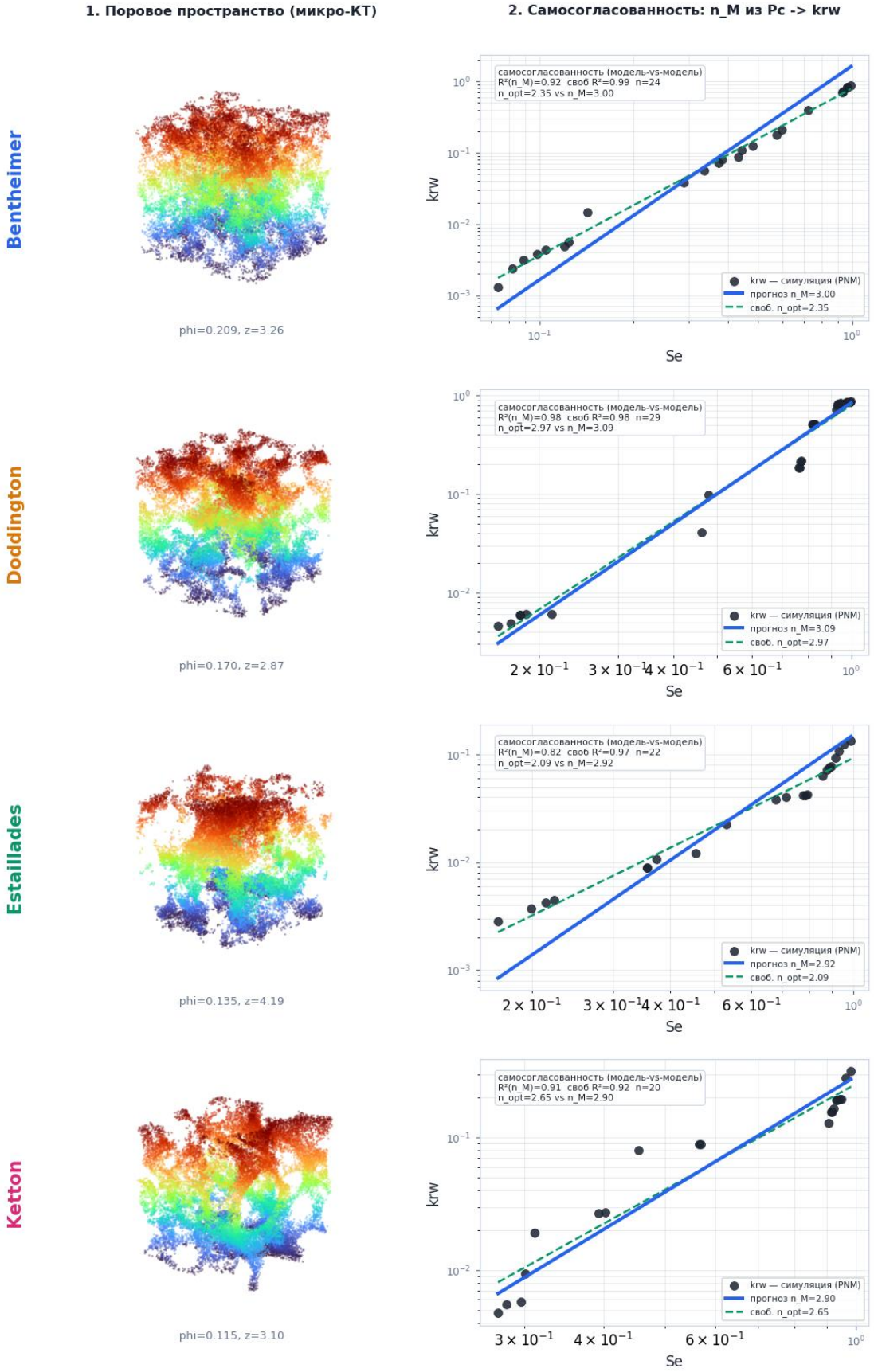

Figure 3. Consistency of the model-free exponent on digital rocks (Imperial College repository [24, 25]). For each of the four lithologies, a representative REV-scale subvolume is

shown, having passed quality control on both $P_c$and $k_{rw}(\lambda \leq 5)$. **(a)** 3D pore-space geometry. **(b)** Relative permeability of the wetting phase k_{rw}: points — pore-network simulation (OpenPNM) on the same network; solid line — prediction $k_{rw} = A\, S_e^{n_M}$with the exponent $n_M$taken from the $P_c$curve and scale factor A. The agreement between $n_M$and $n_{BC}(|\,\Delta\,| \leq 0.20)$ and the prediction quality ($R^2_{\log} = 0.82$–0.98) confirm self-consistency. $P_c$and $k_{rw}$are computed on identical geometry.

Finally, the range-invariant moment law is verified on the full combined sample of 283 real P_c curves. The fit-free moment-based estimate

$$n_M \approx \tau + 2 + 2\,\frac{\mathrm{SD}(\ln P_c)}{\mathrm{SD}(\ln S_e)} \tag{9}$$

reproduces the exact spectral exponent with $R^2 \approx 0.87$, confirming that the exponent is governed primarily by the relative width of the distribution of the logarithm of capillary pressure, σ_w/σ_x (here $w = \ln P_c$), rather than by local features of the curve's shape. The factorization $n_M = \tau + 2\rho_{xy}\,\sigma_y/\sigma_x$ admits a physical interpretation: the effective relative-permeability exponent is twice the mean logarithmic slope of the normalized capillary-conductivity integral, uniting Mualem's integral approach and the Brooks–Corey power-law parameterization within a single closed-form construction. This construction provides a physical justification for a well-known empirical heuristic in petrophysics, according to which the accuracy of a power-law approximation of relative permeability is controlled predominantly by the slope n, with a free scale factor A, while subtle variations in the shape of the P_c curve are masked by this freedom. Crucially, unlike the heuristic — which applies only after the fact, once the k_r points have already been measured — the factorization computes the required slope a priori, directly from the shape of the P_c curve, thereby turning a qualitative observation into a closed-form predictor with an analytically defined accuracy limit.

One of the results of this study is the quantitative determination of the limit of predictability of k_r from P_c. On the sample of ≈ 283 real specimens, it is established that the P_c curve determines the relative-permeability exponent only up to a sample-specific residual $r = n_{opt} - n_M$. The gap to the freely fitted exponent amounts to $\Delta R^2_{\log} \approx 0.11$ on the UNSODA dataset and ≈ 0.04 on Dataset A. This gap is eliminated neither by introducing spectral curvature (the quadratic term of a log–log expansion of the kernel), nor by a percolation correction, nor by a global recalibration of the tortuosity parameter τ. The residual $r$is not random noise. After controlling the false discovery rate via the Benjamini–Hochberg procedure and using partial correlation controlling for λ, it retains a statistically significant dependence on grain-size composition (the clay, silt, and sand fractions). A direct connectivity check on the digital rocks confirmed the equivalence $n_M \approx n_{BC}$ at the rock scale.

The sign of this dependence — on clay-rich media, the exponent n_M turns out to be lower than optimal — is consistent with the hypothesis of an additional

contribution from film flow and bound water to the conductivity of the wetting phase, i.e., with a role for the topological connectivity of the pore space beyond the contribution of pore size alone. Within a given dataset, the residual is partially recoverable: a priori inclusion of the clay fraction as a connectivity-characterizing variable, under nested cross-validation, closes about 24% of the gap to the ceiling ($p < 0.001$). With nested selection from the full available feature set, the gain is more modest — about 6%. No globally transferable correction between independent datasets could be identified: recalibration of the λ-offset between Datasets A and B is statistically insignificant in either direction (permutation test), and textural descriptors are available in only one of the two datasets.

The resulting decomposition of the relative-permeability exponent takes the form

$$n_{\mathrm{opt}} = \underbrace{n_M}_{\text{retention}} + \underbrace{r}_{\text{connectivity}},$$

where n_M is determined solely by the shape of the P_c curve, while the structural term r is real, is locally recoverable from grain-size descriptors, but as yet lacks a transferable parametric form. The consistency of the sign of the dependence of r on medium composition across different datasets, combined with the non-transferability of its magnitude, points to a robust physical mechanism whose parameterization requires direct structural information about the pore space.

The spectral-moment expansion places the classical exponent $n_{BC} = \tau + 2 + 2/\lambda$ as the leading term of an exact law, whose higher-order terms capture the deviation of the curve's shape from a power law through the moments of P_c, with analytically closed-form, non-fitted coefficients. The leading term $2\sigma_w/\sigma_x$ carries the bulk of the exponent's variability ($R^2 \approx 0.87$), and the statistically significant relationship between the shape-residual and the invariant Brooks–Corey signature confirms the structure of the expansion. It is essential, however, to clearly distinguish two directions of refinement: the moment-based generalization refines the internal structure of the leading term n_M, but does not shift the predictability limit. In terms of k_r prediction quality, the exponent n_M remains equivalent to the Brooks–Corey model. The structural residual r is inaccessible from the moments of the P_c curve, because the moment-based generalization and the connectivity term are orthogonal directions of refinement: the former operates within the space of P_c functions, while the latter requires independent structural information about the pore space.

The results obtained refine and generalize several lines of prior research. The qualitative conclusion of Li and Horne [34] regarding the limited predictive power of capillary-based k_r estimates is here given precise quantitative form, as the measured limit $\Delta R^2_{\log} \approx 0.11$. In contrast to the critical-path approach of Ghanbarian and co-authors [22], which reconstructs the entire k_{rw} curve through a fitted log-normal pore-size distribution, a critical percolation radius, and a set of structural parameters, the proposed method targets a single quantity — the exponent n_M —

without postulating a pore-size distribution shape and without any percolation parameters, leaving the scale factor Aas the sole calibrated parameter. The relationship established in [22] between the connectivity exponent and the critical percolation exponent is consistent with the structural nature of the residual $r$found here. This work's contribution in this respect is that this relationship is isolated in clean form, as the residual $r = n_{\text{opt}} - n_M$, unmixed with the relative-permeability exponent itself, and is statistically evaluated. Its significance is established with false-discovery-rate control via the Benjamini–Hochberg procedure, and its reproducibility is confirmed on an independent (held-out) sample. The structural character of the residual implies that the missing information about pore-space connectivity can, in principle, be recovered from digital core analysis data [10, 11, 24, 25], which points toward a hybrid predictor combining the model-free exponent n_M with topological descriptors derived from pore images.

The closed-form sensitivity (7) is confirmed by direct comparison with the finite-difference derivative of the Buckley–Leverett recovery factor, in the reduction with fixed $k_{ro}(a_{o,f} = 0)$: at $S_{wc} = S_{or} = 0.20$ and $\mu_o/\mu_w = 5$, the analytical and numerical values agree to the third decimal place — $\partial RF_{bt}/\partial n = 0.1535$ versus 0.1537 at $n = 2.0$; 0.0545 versus 0.0545 at $n = 3.5$; 0.0298 versus 0.0298 at $n = 5.0$.

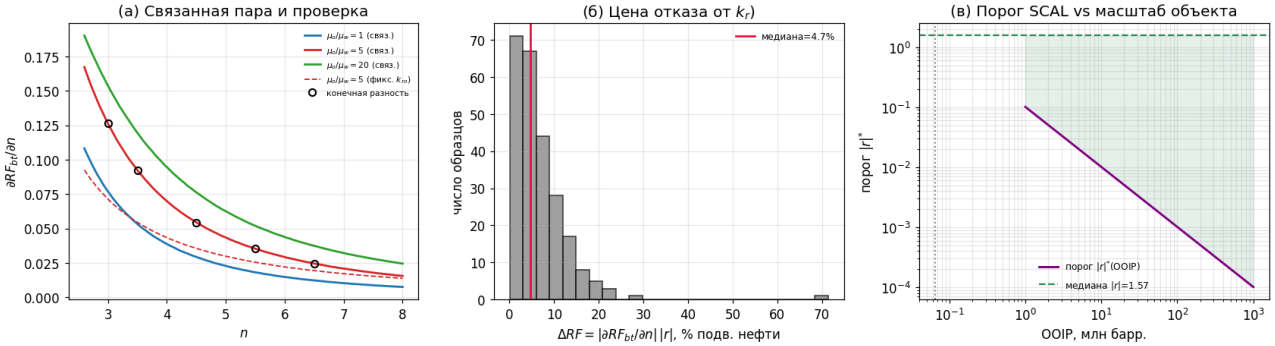

Figure 4. Sensitivity of the water-free oil recovery factor to the relative-permeability exponent. **(a)** The closed-form expression $\partial RF_{bt}/\partial n$(solid lines) for three oil–water viscosity ratios μ_o/μ_w, verified against the finite-difference derivative of the Buckley–Leverett recovery factor (markers) at $\mu_o/\mu_w = 5$with fixed $k_{ro}(a_{o,f} = 0)$. The agreement confirms the analytical derivation (7). **(b)** Distribution of the cost of forgoing laboratory $k_r$measurement, $\Delta RF = |\,\partial RF_{bt}/\partial n\,| \cdot |\,r\,|$, across 245 UNSODA samples; median ≈ 3.8%of movable oil. **(c)** Cost-effectiveness threshold $|\,r^*\,|$as a function of OOIP (green region: where $|\,r\,| > |\,r^*\,|$and SCAL is economically justified).

On the sample of 245 UNSODA specimens, replacing the measured exponent with the model-free n_M shifts the water-free oil recovery factor by, on average (median), $\Delta RF \approx 3.8\%$ of movable oil. This is precisely the cost of forgoing a laboratory k_r measurement, expressed directly as a percentage of recoverable oil. Translating this into the value of a direct measurement yields the SCAL cost-effectiveness threshold:

$$|r^*| = \frac{C_{\mathrm{SCAL}}}{\left|\frac{\partial RF_{bt}}{\partial n}\right| \cdot \mathrm{OOIP} \cdot m_{\text{дв}} \cdot p_{\text{н}}}, \tag{10}$$

where C_{SCAL} is the cost of the testing program, OOIP is the geological (original) oil in place, m_{mob} is the fraction of movable oil, and p_{oil} is the price per barrel. A direct measurement is justified wherever the expected residual exceeds the threshold, $|\, r \,| > |\, r \,|^*$. For a large field (OOIP $= 100$ million bbl, $m_{\mathrm{mob}} = 0.6$, $p_{\mathrm{oil}} = \$70$/bbl), the median value of eliminating the residual is $\Delta V \approx \$1.6 \times 10^8$ at a threshold of $|\, r^* \,| \approx 10^{-3}$. The threshold $|\, r^* \,|$ should be read not as a judgment of whether SCAL is "needed," but as a rule for allocating a finite testing budget.

For the reference Berea sandstone core ($n_M = 4.26$, $n_{\mathrm{opt}} = 4.03$, $r = -0.23$), the coupled sensitivity at $S_{wc} = S_{or} = 0.20$, $\mu_o/\mu_w = 5$, gives $\partial RF_{bt}/\partial n = 0.061$, i.e., $\Delta RF \approx 1.4\%$ of movable oil (≈ 0.84 million bbl at OOIP $= 100$ million bbl, $m_{\mathrm{mob}} = 0.6$; $\approx \$59$ million at \$70/bbl). The coupled estimate exceeds the fixed k_{ro} estimate by 57%.

Propagating the bootstrap-derived statistical spread of the exponent n_M (multiplicative measurement noise in P_c, $\sigma = 0.08$) through the closed-form sensitivity yields a confidence interval for oil recovery directly from a single P_c curve. For Berea sandstone at $\mu_o/\mu_w = 5$: $n_M = 4.26$ [2.85–5.21] propagates to $RF_{bt} =$ 78,4% [65,3; 83,0] of movable oil, with the independently measured $n_{\mathrm{opt}} = 4.03$ giving $RF = 76.9\%$ — within the interval, confirming the consistency of the lab-free prediction. The half-width of the RF interval represents the uncertainty of the recovery prediction from P_c and is compared directly against the threshold $|\, r^* \,|$ and the cost of SCAL. Its asymmetry reflects the saturation of $RF_{bt}(n)$ at large exponents.

Conclusion

A model-free spectral relative-permeability exponent $n_M$has been introduced, computed directly from the capillary pressure curve (Eqs. 1–3) and analytically reproducing the Brooks–Corey model as the limit of perfect correlation, $\rho_{xy} = 1$. The ambiguity in defining the pore-size distribution index is removed by transitioning to the range-invariant ratio σ_w/σ_x, which plays the role of a generalized inverse of the index $1/\lambda$, while the shape-related corrections are rendered operator-invariant. On a sample of approximately 283 real specimens, the exponent achieves a median logarithmic coefficient of determination $R^2_{\log} \approx 0.82$, statistically equivalent to the Brooks–Corey and Burdine models, and does so without fitting any shape parameters. On reservoir core and digital rock models, $R^2_{\log} = 0.82$–0.995 is achieved.

A spectral predictability limit has been quantitatively established: the gap $\Delta R^2_{\log} \approx 0.11$ on the UNSODA dataset is not contained in the P_c curve, and is eliminated neither by introducing spectral curvature, nor by a percolation correction,

nor by recalibrating the tortuosity exponent τ. The residual $r = n_{\text{opt}} - n_M$ is structural, rather than random, in nature, as confirmed by false discovery rate control via the Benjamini–Hochberg procedure and by partial correlation controlling for λ. It is partially recoverable from grain-size composition when the clay fraction is included a priori (nested cross-validation closes about 24% of the gap, $p < 0.001$). A range-invariant, fit-free moment law (Eq. 9) has been obtained, with analytically closed-form correction coefficients, reproducing the exact exponent on 283 real curves with $R^2 \approx 0.87$. Deviation from this law is associated with distance from the invariant Brooks–Corey signature in the skewness–kurtosis plane ($\rho = -0.53$). Direct verification on real reservoir core (Gao et al., 2020; $|\Delta| = 0.068$) and on four digital rock models (mean absolute error 0.13, $R^2_{\log} = 0.82$–0.98) confirms the equivalence $n_M \approx n_{BC}$ at the rock scale and extends the result to problems in digital petrophysics.

Taken together, these results give petrophysics and oilfield development a closed chain $P_c \to n_M \to k_r \to RF$, in which the oil recovery prediction is built directly from readily available capillary pressure data, bypassing costly core-flooding studies. The practical value lies not only in the availability of such a prediction, but in the quantitative assessment of its accuracy, expressed in engineering and economic terms. The proposed method has a low barrier to practical adoption. It is implemented as a computational post-processing module applied to already-available P_c curves and requires neither new laboratory equipment, nor additional core material, nor training datasets. The computational algorithm is not resource-intensive and can be embedded in petrophysical software (Techlog, Geolog, IP) or in a reservoir simulator preprocessor at the stage of specifying saturation functions. A further practical advantage of this work is reproducibility: the model-free exponent is unambiguous and independent of the choice of retention model, whereas the arbitrariness of choosing between Brooks–Corey and van Genuchten approximations is a source of uncontrolled scatter in saturation functions within geological and reservoir simulation models. Removing this arbitrariness is important for reserves auditing and review.

Taken as a whole, the proposed approach provides a basis for the rational allocation of the core-analysis budget, making it possible to forgo a portion of costly $k_r$measurements. The method makes it possible to populate geostatistical and reservoir simulation models with saturation functions in zones covered by capillary pressure measurements but not by the SCAL program, and also enables rapid screening of development scenarios and prioritization of costly flow experiments. A natural direction for future development is a hybrid predictor combining the model-free exponent $n_M$with pore-space image descriptors: such a predictor could close the residual gap to the spectral ceiling while retaining the low cost of the underlying $P_c$curve, thereby bringing lab-free oil recovery prediction closer to field readiness.

References

Purcell W.R. Capillary pressures — their measurement using mercury and the calculation of permeability therefrom // Journal of Petroleum Technology. 1949. Vol. 1, No. 2. P. 39–48. DOI: 10.2118/949039-G.

Burdine N.T. Relative permeability calculations from pore size distribution data // Journal of Petroleum Technology. 1953. Vol. 5, № 3. P. 71–78. DOI: 10.2118/225-G

Childs E.C., Collis-George N. The permeability of porous materials // Proceedings of the Royal Society A. 1950. Vol. 201, № 1066. P. 392–405. DOI: 10.1098/rspa.1950.0068

Mualem Y. A new model for predicting the hydraulic conductivity of unsaturated porous media // Water Resources Research. 1976. Vol. 12, № 3. P. 513–522. DOI: 10.1029/WR012i003p00513

Brooks R.H., Corey A.T. Hydraulic properties of porous media // Hydrology Papers No. 3. Fort Collins: Colorado State University, 1964. 27 p.

van Genuchten M.Th. A closed-form equation for predicting the hydraulic conductivity of unsaturated soils // Soil Science Society of America Journal. 1980. Vol. 44, № 5. P. 892–898. DOI: 10.2136/sssaj1980.03615995004400050002x

Duan C., Kang B., Deng R. et al. Relative permeability estimation using mercury injection capillary pressure measurements based on deep learning approaches // Journal of Petroleum Exploration and Production Technology. 2024. Vol. 14. P. 1933–1951. DOI: 10.1007/s13202-024-01826-3

Ji L., Xu F., Lin M. et al. Rapid evaluation of capillary pressure and relative permeability for oil–water flow in tight sandstone based on a physics-informed neural network // Journal of Petroleum Exploration and Production Technology. 2023. Vol. 13. P. 2499–2517. DOI: 10.1007/s13202-023-01682-7

Moodie N., McPherson B. An integrated approach to derive relative permeability from capillary pressure // Computational Geosciences. 2024. Vol. 28, № 4. P. 755–770. DOI: 10.1007/s10596-024-10297-8

Liu S., Fan M., Lu D. Uncertainty quantification of the convolutional neural networks on permeability estimation from micro-CT scanned sandstone and carbonate rock images // Geoenergy Science and Engineering. 2023. Vol. 230. Art. 212160. DOI: 10.1016/j.geoen.2023.212160

Meng Y., Jiang J., Wu J., Wang D. Transformer-based deep learning models for predicting permeability of porous media // Advances in Water Resources. 2023. Vol. 179. Art. 104520. DOI: 10.1016/j.advwatres.2023.104520

Cao L., Jiang F., Chen Z. et al. Data-driven interpretable machine learning for prediction of porosity and permeability of tight sandstone reservoir // Advances in Geo-Energy Research. 2025. Vol. 16, № 1. P. 21–35. DOI: 10.46690/ager.2025.04.04

Lanetc Z., Zhuravljov A., Armstrong R.T. et al. Estimation of relative permeability curves in fractured media by coupling pore network modelling and volume of fluid methods // International Journal of Multiphase Flow. 2024. Vol. 171. Art. 104668. DOI: 10.1016/j.ijmultiphaseflow.2023.104668

Foroughi S., Bijeljic B., Gao Y., Blunt M.J. Incorporation of sub-resolution porosity into two-phase flow models with a multiscale pore network for complex microporous rocks // Water Resources Research. 2024. Vol. 60, № 5. Art. e2023WR036393. DOI: 10.1029/2023WR036393

Zhao X., Shi B., Wang X. et al. Modeling of permeability and formation factor of carbonate digital rocks: dual-pore-network and pore-network-continuum models // Transport in Porous Media. 2025. Vol. 152, № 2. Art. 37. DOI: 10.1007/s11242-025-02177-1

Liu Y., Gong W., Zhao Y., Jin X., Wang M. A pore-throat segmentation method based on local hydraulic resistance equivalence for pore-network modeling // Water Resources Research. 2022. Vol. 58, № 12. Art. e2022WR033142. DOI: 10.1029/2022WR033142

Zhang G., Foroughi S., Raeini A.Q., Blunt M.J., Bijeljic B. The impact of bimodal pore size distribution and wettability on relative permeability and capillary pressure in a microporous limestone

with uncertainty quantification // Advances in Water Resources. 2023. Vol. 171. Art. 104352. DOI: 10.1016/j.advwatres.2022.104352

Aslannezhad M., Sayyafzadeh M., Tang D. et al. Upscaling relative permeability and capillary pressure from digital core analysis in Otway formation: considering the order and size effects of facies // Gas Science and Engineering. 2024. Vol. 128. Art. 205363. DOI: 10.1016/j.jgsce.2024.205363

Matthai S.K., Tran L.K. Numeric determination of relative permeability of heterogeneous porous media with capillary discontinuities // Advances in Water Resources. 2023. Vol. 175. Art. 104430. DOI: 10.1016/j.advwatres.2023.104430

AL-Dujaili A.N., Shabani M., AL-Jawad M.S. Effect of heterogeneity on capillary pressure and relative permeability curves in carbonate reservoirs. A case study for Mishrif formation in West Qurna/1 oilfield, Iraq // Iraqi Journal of Chemical and Petroleum Engineering. 2023. Vol. 24, № 1. P. 13–26. DOI: 10.31699/IJCPE.2023.1.3

Bagherabadi P., Moradi B., Rasaei M.R. Gaining pore-scale insights into relative permeability curves of two-phase flows in porous media: a modified LBM study // Computational Geosciences. 2025. Vol. 29. Art. 45. DOI: 10.1007/s10596-025-10384-4

Ghanbarian B., Ioannidis M.A., Hunt A.G. Theoretical insight into the empirical tortuosity-connectivity factor in the Burdine–Brooks–Corey water relative permeability model // Water Resources Research. 2017. Vol. 53, № 12. P. 10395–10410. DOI: 10.1002/2017WR021753

Nemes A., Schaap M.G., Leij F.J., Wösten J.H.M. Description of the unsaturated soil hydraulic database UNSODA version 2.0 // Journal of Hydrology. 2001. Vol. 251, № 3–4. P. 151–162. DOI: 10.1016/S0022-1694(01)00465-6

Blunt M.J., Bijeljic B., Dong H. et al. Pore-scale imaging and modelling // Advances in Water Resources. 2013. Vol. 51. P. 197–216. DOI: 10.1016/j.advwatres.2012.03.003

Andrä H., Combaret N., Dvorkin J. et al. Digital rock physics benchmarks — Part I: Imaging and segmentation // Computers & Geosciences. 2013. Vol. 50. P. 25–32. DOI: 10.1016/j.cageo.2012.09.005

Valvatne P.H., Blunt M.J. Predictive pore-scale modeling of two-phase flow in mixed wet media // Water Resources Research. 2004. Vol. 40, № 7. Art. W07406. DOI: 10.1029/2003WR002627

Buckley S.E., Leverett M.C. Mechanism of fluid displacement in sands // Transactions of the AIME. 1942. Vol. 146. P. 107–116. DOI: 10.2118/942107-G

Welge H.J. A simplified method for computing oil recovery by gas or water drive // Journal of Petroleum Technology. 1952. Vol. 4, № 4. P. 91–98. DOI: 10.2118/124-G

Tuli A., Hopmans J.W. Effect of degree of fluid saturation on transport coefficients in disturbed soils // European Journal of Soil Science. 2003. Vol. 55, № 1. P. 147–164. DOI: 10.1046/j.1365-2389.2003.00493.x

Assouline S., Or D. Conceptual and parametric representation of soil hydraulic properties: a review // Vadose Zone Journal. 2013. Vol. 12, № 4. P. 1–20. DOI: 10.2136/vzj2013.07.0121

Richardson J.G., Kerver J.K., Hafford J.A., Osoba J.S. Laboratory determination of relative permeability // Petroleum Transactions, AIME. 1952. Vol. 195. P. 187–196. DOI: 10.2118/952187-G

Pini R., Benson S.M. Simultaneous determination of capillary pressure and relative permeability curves from core-flooding experiments with various fluid pairs // Water Resources Research. 2013. Vol. 49, № 6. P. 3516–3530. DOI: 10.1002/wrcr.20274

Gao Y., Raeini A.Q., Selem A.M., Bondino I., Blunt M.J., Bijeljic B. Pore-scale imaging with measurement of relative permeability and capillary pressure on the same reservoir sandstone sample under water-wet and mixed-wet conditions // Advances in Water Resources. 2020. Vol. 146. Art. 103786. DOI: 10.1016/j.advwatres.2020.103786

Li K., Horne R.N. Comparison of methods to calculate relative permeability from capillary pressure in consolidated water-wet porous media // Water Resources Research. 2006. Vol. 42, № 6. Art. W06405. DOI: 10.1029/2005WR004482

Tyler S.W., Wheatcraft S.W. Fractal processes in soil water retention // Water Resources Research. 1990. Vol. 26, № 5. P. 1047–1054. DOI: 10.1029/WR026i005 P. 1047–1054

Meer D.J., Weeks E.R. Bounded distributions place limits on skewness and larger moments // PLOS ONE. 2024. Vol. 19, № 2. Art. e0297862. DOI: 10.1371/journal.pone.0297862

About the Author

Elena M. Avraham – Candidate of Physical and Mathematical Sciences, Associate Professor of the Department of Computer Technologies and Systems of the Kuban State Agrarian University named after I.T. Trubilin
13, Kalinina st., Krasnodar, 350044, Russian Federation
e-mail: av.el3@yandex.com